Ophthalmologic Image Registration Based on Shape-Context: Application to Fundus Autofluorescence (FAF) Images

Adnan Rashid Chaudrhy, Jean-Claude Klein, Estelle Parra-Denis

Ophthalmologic Image Registration based on shape-context: Application to Fundus Autofluorescence (FAF) images

A.R. CHAUDHRY, J.C. KLEIN, E. PARRA-DENIS
Centre de Morphologie Mathématique
Ecole des Mines de Paris

Abstract

A novel registration algorithm, which was developed in order to facilitate ophthalmologic image processing, is presented in this paper. It has been evaluated on FAF images, which present low Signal/Noise Ratio (SNR) and variations in dynamic grayscale range. These characteristics complicate the registration process and cause a failure to area-based registration techniques[1, 2]. *Our method is based on shape-context theory* [3]. *In the first step, images are enhanced by Gaussian model based histogram modification. Features are extracted in the next step by morphological operators, which are used to detect an approximation of vascular tree from both reference and floating images. Simplified medial axis of vessels is then calculated. From each image, a set of control points called Bifurcation Points (BPs) is extracted from the medial axis through a new fast algorithm. Radial histogram is formed for each BP using the medial axis. The Chi2 distance is measured between two sets of BPs based on radial histogram. Hungarian algorithm is applied to assign the correspondence among BPs from reference and floating images. The algorithmic robustness is evaluated by mutual information criteria between manual registration considered as Ground Truth and automatic one.*

Keywords: *Fundus autofluorescence, area-based registration, shape-context, histogram modification, bifurcation points and mutual information.*

1 Introduction

In this paper, we present an automatic registration technique based on shape context theory [3]. The shape context is a feature-based method [4, 5] working on extracted features called as control points (CPs), which are silent, distinct and well spread all over the image [6, 7]. Examples of features are points (corners, crossing and high curvature points on shape), lines and regional features [8].

In feature-based methods, similarity measure is maximized between corresponding features extracted from two images, the reference image and the floating image. There are three different matching settings, an intensity match in a closed neighborhood around the features [9], geometrical inter-distribution [10, 11] and symbolic description of features [12].

The proposed method is based on extraction of variants of vessel crossing used as CPs from both reference and floating images with different dynamics of matching as in [6, 7, 12-14]. Similar to [9] correlation is measured around CPs [6]. In [14], sequential fundus images alignment could be done by using the sum of the absolute values of the differences (SAVD) method. Bayesian Hough transform is used and a precise affine estimate is computed for most likely transformations for registration [12]. In [13], the scheme described in this paper combined the closest interval criterion between un equal number of corresponding feature points with SVD algorithm to accurately register retinal images. The performance of feature based registration methods is dependent on the accuracy of correspondences. Recently, hybrid technique based on both area based and features based methods are appearing in retinal image registration [2]. Shape context method can be seen as a hybrid method as it deals with information at CPs containing rich information about its neighborhood.

In the present study we applied image registration algorithms on FAF images. In fact, FAF imaging has shown to be useful in retinal diseases for diagnosis, documentation of disease progression, and monitoring of novel therapies. Moreover FAF images present important noise, low SNR and important variation on its grey scale range. It presents limitation to classical retinal image registration techniques used.

Firstly, properties and acquisition of FAF image modality are presented. Secondly, the different steps of the proposed registration method are divided in three parts: the pre-treatment (based on contrast enhancement), and the pattern recognition (features detection and control points extraction, the correspondence between control points and estimation of alignment transformation by means of shape matching technique. Lastly, the evaluation of the algorithm using mutual information criteria is detailed. The Figure 1 summarizes the proposed registration algorithm for FAF images.

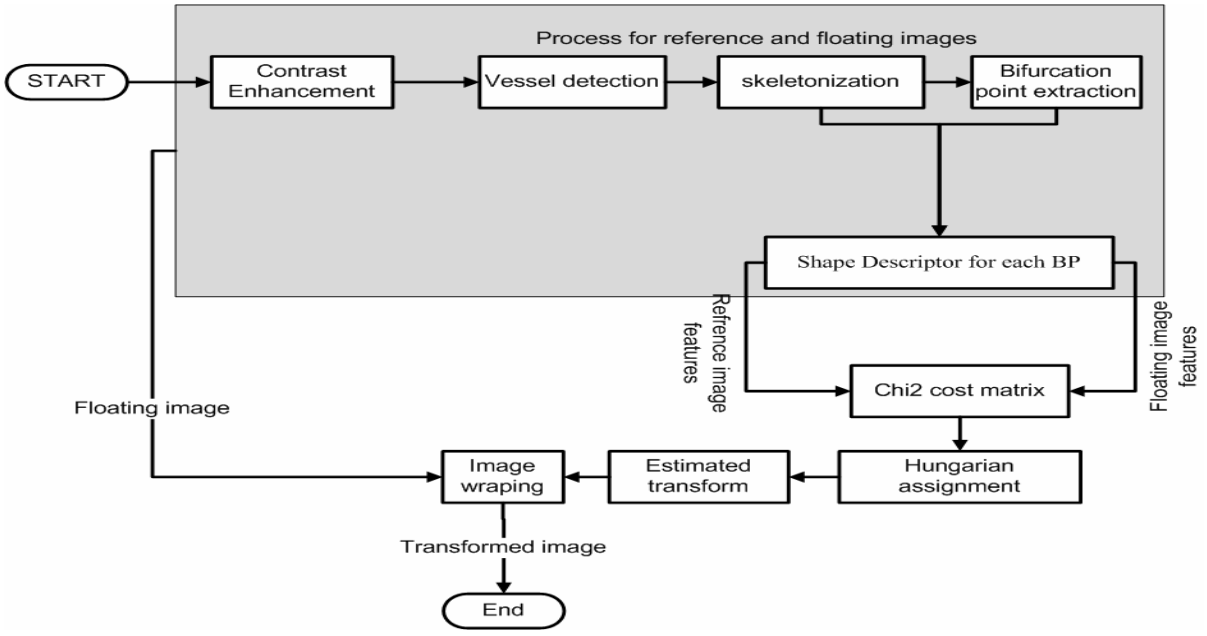

Figure 1 Flow chart shows the various steps of registration algorithm.

2 *FAF images acquisition and characteristics*

The FAF images of the retina are obtained with an angiograph equipped with a scanning laser of 488 nm wavelength (Scanning Laser Ophthalmoscope (SLO)). The autofluorescence is emitted by the presence of a pigment (lipofuscin) in retinal pigment epithelium, which is a good indicator of the retinal activity. Field of view is 30°, which almost encompasses the posterior pole of retina. During the patient examination, a sequence of FAF images is acquired. Each sequence is 3-10 seconds in length with sampling rate of 18 frame/sec. Individual images are monochrome and digitized with pixel resolution of 768×768 . The SNR of individual FAF images is very low and variation of dynamic grayscale range is introduced by manual image acquisition process. To obtain an exploitable image it is necessary to register several images of the sequence and to calculate their average. This is the main application of the proposed algorithm.

3 *Proposed image registration method*

3.1 *Pre-treatment: Contrast Enhancement*

As mention before, FAF images show variation in dynamic greyscale range during image acquisition process. This variation is common between successive examinations of patients on the same SLO. Thus, there is a need to standardize the contrast that improves the efficiency of higher level image processing algorithm. Linear Contrast Stretch (LCS) and Histogram Equalization (HE) are the two basic contrast enhancement methods [15].
LCS requires iterative changes to greyscale range form image to image. In the same manner, the effect of HE is harsh by amplification of noise. It is common observation in FAF images that although dynamic range varies it shows a similar histogram shape i.e. distribution of grey values.

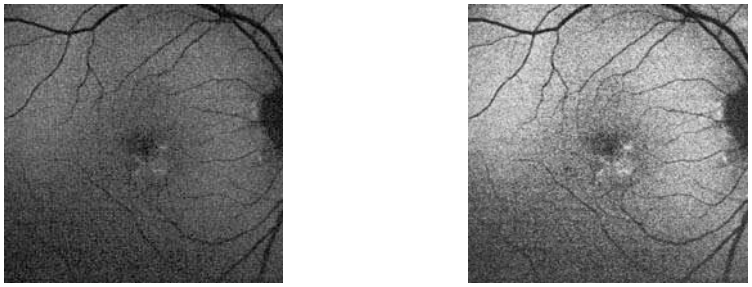

a) Raw FAF image **b) Contrast enhancement of (a)**

Figure 2 Histogram modification under Gaussian model

Considering the natural shape of FAF image histogram, A Gaussian model of histogram distribution over 255 grey scales is calculated by

$$G(x) = \frac{N}{\sigma} \exp^{-\frac{(x-m)^2}{2\sigma^2}}$$

Where, m is the mean, N the number of pixels and $x = 0, ..., 255$. Mean and standard deviation gives two degrees of freedom for Gaussian model of histogram distribution. The details of histogram modification is available in [15].

FAF images with better contrast usually have a mean of approximately 115 and standard deviation of about 72 and these values are used for contrast enhancement. The result is standardization of dynamic grayscale range and better contrasted images. Modified FAF images have blood vessels, papilla, macula and lesions more visible than in original images. Furthermore images are more pleasant in appearance Figure 2 (b).

3.2 *Pattern recognition: Feature detection and extraction of control points*

Segmented blood vessels play an important role in many medical applications for diagnosis and registration of patient images taken at different examinations. Including these well known applications, they also help in detection of other anatomical structure and lesions. Naturally, segmentation methods depend on image modality, application domain and they exploit the properties of vascular structure in a modality. Vessel segmentation algorithms are categorized into a wide variety of techniques as in review [16] particularly for retinal blood vessels extraction, match filter [17], neural networks [18] and mathematical morphology [12, 19] based methods are proposed. In FAF images, blood vessels are the most distinctive feature of retinal image, also exhibits characteristics of diameter less than 15 pixels in image size of 768×768, elongated shape, darker than background as monochrome modality, tortuosity, piecewise linear and appear as a tree like structure originating from papilla. Furthermore, vascular structure is encompassing whole of fundus, thus making it suitable choice for search of control points [7, 11, 12].

3.2.1 Vessels Extraction

In the light of above mention properties of vessels in FAF images, we present a fast and robust technique for vascular tree extraction. The algorithm is based on mathematical morphological operators [20, 21]. Histogram modified image still has low SNR. Image is filtered with a Gaussian filter (5x5) to remove small noise peaks, causing discontinuity in blood vessels extraction. Black details are enhanced by successive morphological erosion with hexagonal structuring elements [21]. Excessive noise is attenuated and small black details are removed while preserving the crucial vascular tree. When the size of Gaussian filter increases (more than 5x5), we observe a discontinuity between vessels, while increasing the size of erosion will displace the vessels contour. A black top-hat is applied to enhance the contrast of large and elongated structure with a structuring element of size greater than the diameter of the largest vessel. Binary image is obtained by thresholding black top-hat image with threshold λ. The threshold value is selected automatically, by first order statistical property of top-hat i.e. mean grey scale. An area-thresholding of small size is applied to remove small elongated noise particles. Whole filling and closing is applied to remove small holes and discontinuities in extracted blood vessels. The Figure 3 shows the steps of feature extraction algorithm.

Skeletonization transformation is applied to extract the medial axis of vascular structure. The category of skeletonization utilized here is defined by thinning approaches Zhang and Sue [22]. Motivations for the skeletonization is the need to simplify the shape of an object (approximate vessels extracted) in order to find BPs for the matching algorithm. There exist small undesirable branches and bubbles, which are removed by an efficient skeletal branch filtering algorithm. This refined medial axis of vascular structure is used to extract the BPs explained in the next section.

3.2.2 Bifurcation points

The BPs are the points, where two or more vessels intersect. They appear as a big vessel subdivided into smaller branches and also by crossing of arteries over veins. A new method of calculating BPs is proposed based on the counting of the distinct branches associated with a pixel rather than just analyzing the neighboring pixels. If there exist more than two branches then the point is termed as BP as shown in Figure 4 (a). The BPs are easily determined from the skeleton. This detection is not sensible to the noise present in FAF image.

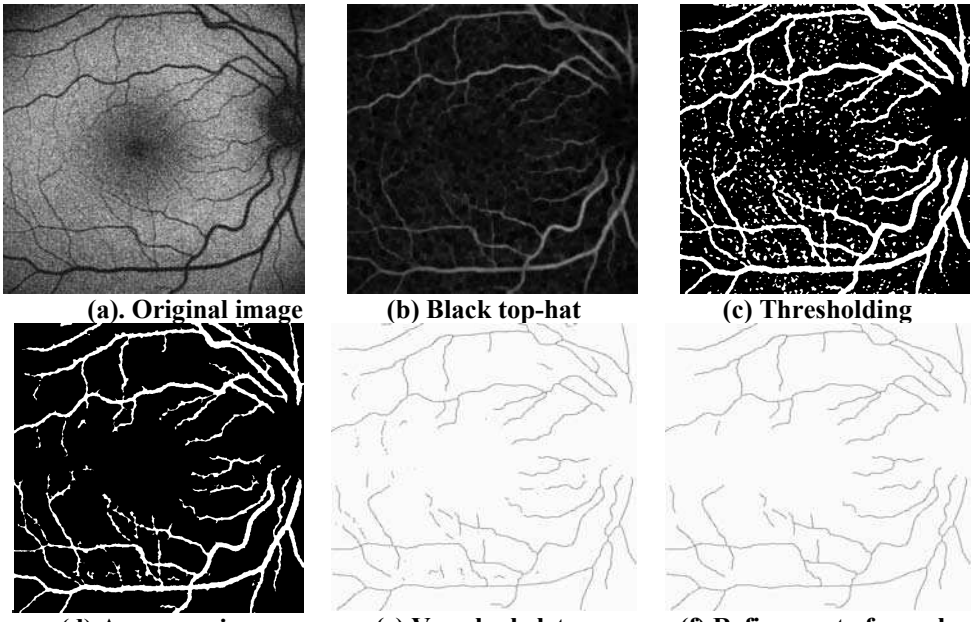

(a). Original image (b) Black top-hat (c) Thresholding

(d) Area-opening (e) Vessels skeleton (f) Refinement of vessels skeleton

Figure 3. Steps of vessels detection.

3.3 *Shape context*

Shape matching is an approach to exploit the similarity between two shapes. In the context of shape matching, a state of art work has been realized in [3] and various shape matching techniques are reviewed in [23]. In this section, we propose to utilize frame work of shape matching [3] by calculating the shape descriptors around each BP in two successive images of the FAF sequence, giving us a set $CP = \{cp_1, cp_2, ..., cp_m\}$ included in $P = \{p_1, p_2, ..., p_n\}$ with $cp_l, p_i \in \mathbb{R}^2$. As the full vessel contour relative descriptor will be rich and matching will be easy but computationally expensive, thus we experimented with the BPs and concluded that discriminative descriptors extracted around the BPs are robust. For a point p_i on the shape, we find the course histogram h_i of the relative coordinates of the m points in a zone. The zone is described by log distance.

$$h_i = \#\{q \neq p_i \quad : \quad (q - p_i) \in bin(k)\}$$

The histogram h_i defines the shape around control point cp_k in a zone. We use bins that are uniform in log-polar space, making it more sensitive to near points rather than far away points. Let us consider a point p_i on the first shape and a point q_i on the second shape. Let $C_{ij} = C(p_i, q_i)$ denotes the cost of matching these two points. As shape contexts are distributions represented as histograms, it is natural to use the Chi 2 statistic test:

$$C_{ij} = C(p_i, q_i) = \frac{1}{2} \sum_{k=1}^{K} \frac{\left[h_i(k) - h_j(k)\right]^2}{h_i(k) + h_j(k)}$$

Where $h_i(k)$ and $h_j(k)$ denoted the K-bin normalized histogram at p_i and q_i, respectively.

Given the set of costs C_{ij} between the pairs of control points p_i, on the first shape and q_i on the second shape, we want to minimize the total cost of matching. Subject to the constraint that matching is one to one i.e. π is a permutation. This is an instance of the square assignment problem, which can be solved in $O(N^3)$ using the Hungarian method [24].

$$\begin{bmatrix} 0 & 0 & 0 & 0 & 0 & 2 & 0 & 0 & 0 & 0 & 0 & 0 \\ 0 & 0 & 0 & 0 & 0 & 0 & 0 & 0 & 0 & 0 & 0 & 0 \\ 1 & 1 & 0 & 0 & 0 & 2 & 0 & 1 & 0 & 0 & 0 & 0 \\ 1 & 1 & 0 & 0 & 0 & 1 & 0 & 0 & 0 & 0 & 0 & 0 \\ 0 & 1 & 0 & 0 & 0 & 1 & 0 & 0 & 0 & 0 & 0 & 0 \\ 0 & 2 & 0 & 0 & 0 & 2 & 0 & 0 & 0 & 1 & 0 & 1 \\ 0 & 3 & 0 & 0 & 0 & 3 & 0 & 0 & 0 & 1 & 0 & 3 \\ 0 & 6 & 0 & 0 & 0 & 7 & 0 & 0 & 0 & 5 & 0 & 0 \\ 0 & 6 & 0 & 7 & 0 & 8 & 0 & 0 & 0 & 10 & 0 & 0 \\ 11 & 0 & 0 & 10 & 0 & 16 & 0 & 0 & 0 & 17 & 0 & 0 \\ 34 & 0 & 0 & 0 & 0 & 24 & 0 & 0 & 0 & 26 & 0 & 0 \\ 9 & 0 & 0 & 0 & 0 & 72 & 0 & 0 & 0 & 62 & 0 & 44 \end{bmatrix}$$

a). Radial Histogram over BP **b) Radial histogram**

Figure 4 Shape based discriminant features around a bifurcation point.

In our experiment the radial histogram is divided into 12 distance bins and 12 angular bins thus forming a descriptor of 144 bins and a radial size of 100 pixels, which has sufficient discriminatory information for correct correspondence, as shown in Figure 4. The result of correspondence includes false matches, which are refined by statistical analysis of motion vectors based on median and BPs rejected in cost analysis but falling within acceptable motion are reintroduced.

3.4 Modeling transformation

In the previous section, we had a finite set of point correspondences between two images of FAF sequence. One can proceed to estimate a plane transformation $T = \mathbb{R}^2 \to \mathbb{R}^2$ that can be used to map points from floating image to reference image. The motivation is to look for a correct transformation that can account for eye movements, and for small rotational and translational changes introduced by movement on the chin holder during the FAF image acquisition process. In literature, transformation model of different dimensions are available, estimation of a suitable translation transform in [25, 26], rigid body transformation in [27], an affine model which accounts for scale and shear as in [28, 29] or complicated transformations based on thin-plate splines [30] or polynomial transforms [31].

In our application, a global affine transformation model is applied and found to be accommodating within the 6 degree of freedom. Considering, we have a set of homogenous points $P^3 = \{p_1, p_2, ...p_m\}$ from reference image to $Q^3 = \{q_1, q_2, ...q_m\}$ in floating image, then

$$P_{3\times 1} = A_{3\times 3} Q_{3\times 1} \qquad \begin{pmatrix} p_x \\ p_y \\ 1 \end{pmatrix} = \begin{pmatrix} m_0 & m_1 & m_2 \\ m_3 & m_4 & m_5 \\ 0 & 0 & 1 \end{pmatrix} \begin{pmatrix} q_x \\ q_y \\ 1 \end{pmatrix}$$

$A_{3\times 3}$, is the affine matrix mapping, point q_i on to p_i .Forward transform is calculated by matrix multiplying $Q_{3\times m}$ with pseudo-inverse of $P_{3\times m}$.

$$forward \quad transform: A^f{}_{3\times 3} = Q_{3\times m} P^{-1}{}_{3\times m}$$

and backward transformation matrix A^r is given,

$$backward \quad transform: A^r{}_{3\times 3} = inv(A^f{}_{3\times 3})$$

In [32], evaluation of different interpolation techniques under registration methods are presented. We have selected bilinear interpolation to estimate values on the discrete reference grid from the $\mathbb{R}$ transformed image space.

4 Results and evaluation

The registration method is trailed over normal FAF image sequences with Heidelberg Angiograph 2. The algorithm was tested on 45 FAF images. A method to measure the accuracy of image registration is to use a measurement Q_MI based on the Mutual information (MI) [5, 28] between the reference image and the transformed floating image and on the MI obtained for a ground truth registration of images of same modality. For example, if we want to register two FAF images, we compare experimental result $MI\left(A, T(B)\right)$ to the result

obtained by a ground truth image matching performed for reference images of the same modality $MI\left(AF, T^{*}(AF)\right)$ and we normalize the result:

$$Q\_MI_{AF}(A,T(B)) = \frac{MI\left(A,T(B)\right) - MI\left(AF,T^{*}(AF)\right)}{MI\left(AF,T^{*}(AF)\right)}$$

$Q\_MI(A,T(B))$ represents the relative deviation between the ground truth registration and the one obtained by automatic registration algorithms. We consider that Q_MI gives a good result if its value lies between $\pm$ 5%.

In fact, many publications show that the value of MI is strongly related to the accuracy of the applied transformation. The well registered the images are, the more important value of MI is measured, around the good transformation MI shows a sharp increasing pick.

On Figure 5, we present the result of the mean of two images extracted from a FAF sequence. The right hand image correspond to an unregistered image otherwise the left hand image correspond to our registration result. We applied the bi-dimensional distribution of voxel intensity values (or scattered plot histogram) for unregistered and registered images. We noticed MI increases when images are registered. For a non-perfect registration, the value of MI is almost the same that for unregistered images (0.14 in the present case) and the value suddenly increases when we approach the best registration (up to 0.3160). The final result of the registration performed is presented in Figure 5(b).

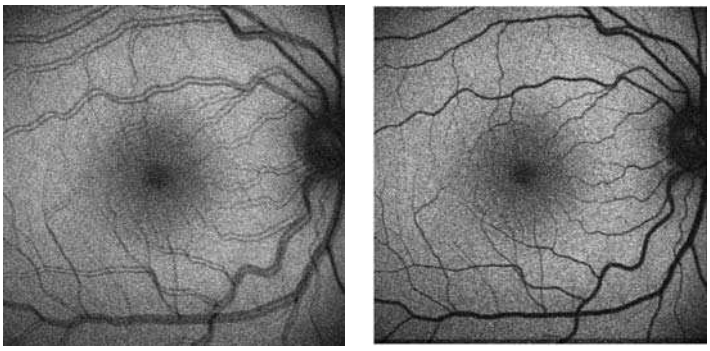

a) Unregistered **b) Registered**

Figure 5 Mean of the two images presented on FAF image pair.

5 Conclusion

The registration algorithm presented deals with the noisiest of the image modality acquired with SLO. The main objective of the experiment is to develop efficient registration technique independent of specific image characteristics in retinal images. In the method, FAF dynamic grayscale range is standardized with Gaussian histogram modal and extra noise is filtered. Method is based on efficient retinal blood vessels detection algorithm and fast algorithm is proposed for extraction of BPs. Vessels shape is explored to define a discriminatory feature around BPs to form a radial histogram. The affine model of transformation is used, which accommodates for temporal changes. The discontinuity of image wrap is improved with bilinear interpolation. The intra-modality registration is of interest as SLO is capable to acquire images in five different modalities that are red-free, indocyanine green (ICG), fluorescein angiography, infra-red and autofluorescence. Each of these modalities plays an important role in the diagnosis of retinal diseases. The registration algorithm efficiently works with FAF images. It is easily extendable for intra-modality registration with changes in vessels extraction module.

References

1. N. Ritter, R. Owens, and J. Cooper, *Registration of Stereo and Temporal Images of the Retina.* IEEE Trans. on Medical Imaging 1999. 18(5): p. 404-418.
2. T. Chanwimaluang, G. Fan, and S. R. Fransen, *Hybrid Retinal Image Registration.* IEEE Trans. on Information Technology in BioMedicine, 2006. 10(1): p. 129-133.
3. S. Belongie, J. Malik, and J. Puzicha, *Matching and Object Recognition Using Shape Contexts.* PAMI, 2002. 24(4): p. 509-522.

4. L. G. Brown, *A Survey of Image Registration Techniques.* ACM Computing Surveys (CSUR), 1992. 24: p. 325-376.
5. Xiao-Hong Zhu, Cheng-Chang Lu, and Yang-Ming Zhu, *Stereo and Temporal Retinal Image Registration by Mutual Information Maximization*, in *Handbook of Biomedical Image Analysis: Registration Models*. 2005, Springer US.
6. A. Can, et al., *A feature-based, robust, hierarchical algorithm for registering pairs of images of the curved human retina.* IEEE Trans. on Pattern Analysis Machine Intelligence., 2002. 24(3): p. 347-364.
7. W. E. Hart and M.H. Goldbaum, *Registering retinal images using automatically selected control point pairs.* Proc. IEEE Int. Conf. on Image Processing,, 1994. 3: p. 576-581.
8. Paul J. Besl and N.D. McKay, *A Method for Registration of 3-D Shapes.* IEEE Trans. on Pattern Analysis and Machine Intelligence, 1992. 14(2).
9. E. Peli, R. A. Augliere, and G. T. Timberlake, *Feature-Based Registration of Retinal Images.* IEEE Trans. on Medical Imaging, 1987. 6(3): p. 272-278.
10. P. Jasiobedzki, *Registration of Retinal Images Using Adaptive Adjacency Graphs.* Proc. of Sixth Annaul IEEE Symposium on Computer-Based Medical Systems., 1993: p. 40-45.
11. W. Aguilar, et al., *Graph-Based Methods for Retinal Mosaicing and Vascular Characterization*, in *Graph-Based Representations in Pattern Recognition*. 2007, Springer Berlin / Heidelberg.
12. F. Zana and J. C. Klein, *A Multimodal Registration Algorithm of Eye Fundus Images Using Vessels Detection and Hough Transform.* IEEE Trans. on Medical Imaging, 1999. 18(5): p. 419-428.
13. Er-Hu Zhang, Yan Zhang , and Tian-Xu Zhang. *Automatic retinal image resgitration based on blood vessels feature point*. in *Proc. of the First Int. Conf. on Machine Learning and Cybernetics.* 2002. Beijing.
14. J. Jy-Haw Yu, Biing-Man Hung, and Chone-Lin Liou, *Fast algorithm for digital retinal image alignment.* Proc. IEEE Ann. Conf. Engineering in Medicine and Biology (EMBS), 1989. 2: p. 374-375.
15. R. C. Gonzales and R. E. Woods, *Digital image processing*. 2 ed. 2002: Prentice-Hall.
16. C. Kirbas and F. Quek, *A review of vessel extraction techniques and algorithms.* ACM Computing Surveys (CSUR) 2004. 36(2): p. 81-120.
17. S. Chaudhuri, et al., *Detection of Blood Vessels in Retinal Images Using Two-Dimensional Matched Filters.* IEEE Trans. on Medical Imaging, 1989. 8(3).
18. C. Sinthanayothin, et al., *Automated localisation of the optic disc, fovea, and retinal blood vessels from digital colour fundus images.* 1999. 83(8): p. 902-910.
19. F. Zana and J.C. Klein, *Segmentation of vessel like patterns using mathematical morphology and curvature evaluation.* IEEE Trans. on Medical Imaging, 2001. 10(7): p. 1010-1019.
20. J. Serra, *Image analysis and mathematical morphology*. Vol. 2. 1998, New York: Academic Press
21. P. Soille, *Morphological Image Analysis: Principles And Applications*. Vol. 2. 2002: Springer:Heidelberg.
22. T. Y. Zhang and C. Y.Suen, *A fast parallel algorithm for thinning digital patterns.* Communications of the ACM, 1984. 27(3): p. 236-239.
23. R. C. Veltkamp and M. Hagedoorn, *State of the art in shape matching*, in *Principles of visual information retrieval* 2000, Springer-Verlag: London, UK p. 87 - 119
24. C. H. Papadimitriou and K. Steiglitz, *Combinatorial optimization: algorithms and complexity* 1982: Prentice-Hall.
25. J. Noack and D. Sutton, *An algorithm for the fast registration of image sequences obtained with a scanning laser opthalmoscope* Physics in Medicine and Biology, 1994. 39: p. 907-915.
26. M. S. Mort and M.D. Srinath, *Maximum likelihood image registration with subpixel accuracy.* Proc. SPIE: Applications Digital Image Processing XI, 1988. 974: p. 38-43.
27. A. M. Mendonca, Aurklio Campilhol, and JosP Manuel Rodrigues Nunes, *A new similarity criterion for retinal image registration.* Proc. of IEEE Int. Conf. on Image Processing, 1994. 3: p. 696-700.
28. A. Collignon, et al., *Automated multi-modality image registration based on information theory.* Proc. of the Int. Conf. on Information Processing in Medical Imaging (IPMI), 1995: p. 263–274.
29. F. Lalibert, L. Gagnon, and Y. Sheng, *Registration and Fusion of Retinal Images: A Comparative Study.* Proc. of 16th Int. Conf. on Pattern Recognition., 2002. 1: p. 715- 718
30. Fred L.Bookstein, *Principal Warps: Thin-Plate Splines and the Decomposition of Deformations.* IEEE Trans. on Pattern Analysis and Machine Intelligence, 1989. 11(6): p. 567-585.
31. R. Szeliski and S. Lavallée, *Matching 3-D anatomical surfaces with nonrigid deformations using octree-splines.* Int. J. Computer Vision, 1996. 18(2): p. 171-191.
32. S. A. Teukolsky, W. T. Vetterling, and B. P. Flannery, *Numerical Recipes in C*. Chap 10. 1992: Cambridge University Press.